



Dynamics of optical vortices in van der Waals materials

YANIV KURMAN,¹ RAPHAEL DAHAN,¹ HANAN HERZIG SHENFUX,² GILLES ROSOLEN,³ ELI JANZEN,⁴ JAMES H. EDGAR,⁴ FRANK H. L. KOPPENS,^{2,5} AND IDO KAMINER^{1,*} 

¹Department of Electrical Engineering, Technion - Israel Institute of Technology, 32000 Haifa, Israel

²ICFO-Institut de Ciències Fotòniques, The Barcelona Institute of Science and Technology, Av. Carl Friedrich Gauss 3, 08860 Castelldefels (Barcelona), Spain

³Micro and Nanophotonic Materials Group, Research Institute for Materials Science and Engineering, University of Mons, 7000 Mons, Belgium

⁴Tim Taylor Department of Chemical Engineering, Kansas State University, Manhattan, Kansas 66506, USA

⁵ICREA-Institució Catalana de Recerca i Estudis Avançats, Passeig Lluís Companys 23, 08010 Barcelona, Spain

*kaminer@technion.ac.il

Received 6 January 2023; revised 14 April 2023; accepted 19 April 2023; published 17 May 2023

Quantized vortices are topological defects found in different two-dimensional geometries, from liquid crystals to ferromagnets, famously involved in spontaneous symmetry breaking and phase transitions. Their optical counterparts appear in planar geometries as a universal wave phenomenon, possessing topologically protected orbital angular momentum (OAM). So far, the spatiotemporal dynamics of optical vortices, including vortex-pair creation and annihilation, has been observed only in Bose–Einstein condensates. Here we observe optical vortices in van der Waals materials and measure their dynamics, including events of pair creation and annihilation. Vortices of opposite OAM are involved in pair creation/annihilation events, and their relative signs determine the surrounding field profile throughout their motion. The vortices are made of phonon polaritons in hexagonal boron nitride, which we directly probe using free electrons in an ultrafast transmission electron microscope. Our findings promote future investigations of vortex phenomena in van der Waals platforms, toward their use for chiral plasmonics, quantum simulators, and control over selection rules in light–matter interactions. © 2023 Optica Publishing Group under the terms of the [Optica Open Access Publishing Agreement](#)

<https://doi.org/10.1364/OPTICA.485120>

1. INTRODUCTION

Optical vortices are points in the light field with non-zero optical orbital angular momentum (OAM) [1]. In these points, the phase is undefined, creating a singularity with zero amplitude and integer values of OAM, which equals the integrated phase of the field (over 2π) in a closed contour around the vortex location [2,3]. Distinguished by dimensionality, two distinct families of optical vortices are known: vortex beams [4] and planar optical vortices [5]. Vortex beams show a plethora of phenomena [6] from stimulated emission depletion (STED) microscopy [7] and optical tweezers [8], through nonlinear optical effects such as vortex solitons [9], to implications for quantum entanglement [10,11] and transfer of angular momentum from light to matter [12].

In planar systems, optical vortices are confined to the 2D plane and evanescently decay in the out-of-plane direction, as famously shown with surface plasmon polaritons [5] and with other guided modes [13]. Their reduced dimensionality led to unique phenomena such as nanotweezers [14], optical skyrmions [15], and manipulation of selection rules in light–matter interactions [16,17]. Much of the research on planar optical vortices is focused on controlling the vortex OAM and location [18–20]. The control is primarily based on engineering the boundary conditions and laser excitation properties (e.g., polarization), even showing

vortices with high OAM [21]. Delicate engineering of the interference of planar waves enabled sub-cycle ultrafast observations of the formation, dissipation, and rotation of individual vortices [21–24] and of topological plasmon vortices (and vortex arrays), as optical analogs to magnetic merons and skyrmions [23,24]. The latter works suggested to use active control of the excitation pulses to “enable the creation, manipulation and annihilation of plasmonic topological spin textures” [23].

Fundamental to the physics of vortices is the conservation of topological OAM in the vortex, implying that vortex pairs can be created or annihilated while maintaining a fixed overall OAM in each process [25]. These conservation laws were probed experimentally in nanophotonic platforms by sweeping over the frequency [26] or polarization [20] of time harmonic (monochromatic) fields. Such approaches provide an indirect analog of the temporal dynamics of vortices, showing that pairs of vortices can be created and annihilated, and change their location for slowly varying continuous wave fields [27].

The temporal dynamics of vortices, especially their creation and annihilation, attracts further interest due to the famous Berezinskii–Kosterlitz–Thouless (BKT) phase transition [28]. These processes were measured on several occasions in various systems such liquid crystals [29]. Nevertheless, in optical systems,

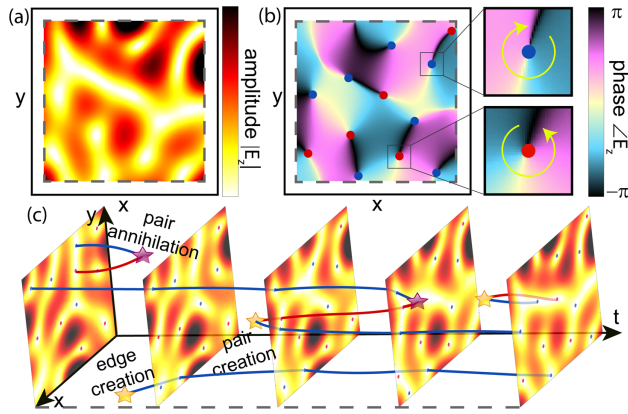


Fig. 1. Theory of planar optical vortex dynamics. Exemplified by a simulation of phonon-polaritons (PhPs) in hexagonal boron nitride (hBN). (a) Simulated PhP electric field amplitude $|E_z|$. (b) Corresponding phase of the field, from which we can determine the locations of the vortices. The vortex locations match the amplitude nodal points. Inset: Blue and red dots denote the location of left-handed and right-handed vortices, respectively. (c) Electric field amplitude as a function of time, marking a few vortex trajectories (blue and red curves) and creation/annihilation events (stars).

the spatiotemporal motion of optical vortices and vortex-pair creation have been measured only in Bose–Einstein condensates [30]. Unlike optical vortex-pair creation, the inverse process of annihilation is less likely due to entropy, which increases the number of vortices in time in a lossy system and, to the best of our knowledge, has remained beyond experimental reach.

In this work, we observe the spatiotemporal dynamics of optical vortices, including events of vortex-pair creation and annihilation, in a van der Waals material in the form of phonon polaritons (PhPs). The planar optical vortices appear as points of zero field amplitude that are shown to move continuously inside the sample. All the features predicted by the theory of vortex temporal dynamics (Fig. 1) are found in our experiments. The OAM of individual vortices is conserved during their movement, and the sum of OAM is conserved during the creation and annihilation of vortex pairs; only on sample edges is the OAM not conserved. Our experiments promote ideas for optical quantum simulators of topological dynamics using van der Waals polaritons.

We use an ultrafast transmission electron microscope (UTEM) [31–37] to probe the spatiotemporal dynamics of PhP vortices in boron-10 isotopically pure hexagonal boron nitride ($h^{10}\text{BN}$). hBN is a widely studied van der Waals material that is polar dielectric and supports PhPs, hybrid modes of photons and optical phonons [38–44]. Besides PhPs in hBN, van der Waals materials span a much larger range of polaritons (including plasmon–polariton, exciton–polariton, and more [45,46]), which have dispersion relations that may be tuned via their thicknesses, surrounding environments, and material doping. Here, PhPs were chosen due to their slow group velocity that determines the vortex velocity and the relatively long lifetime of PhPs in monoisotopic boron $h^{10}\text{BN}$ at room temperature [40,44]. The long lifetime and slow group and phase velocities are essential for showing other planar optical phenomena at room temperature such as PhP cavity dynamics [41] wave packet dynamics [43], and PhP lensing [42].

2. SPATIOTEMPORAL IMAGING OF PLANAR OPTICAL VORTICES USING FREE ELECTRONS

Figure 2 shows how we extract the temporal dynamics of the vortices. We use a pump–probe technique, in which a single laser pulse is divided so that one part is converted to the mid-infrared (IR) regime to pump the PhPs in the sample, while the other part is converted to the UV to excite the free electron probe in the UTEM (see details in Supplement 1, Section S1). Our probing approach is based on the technique called photon-induced near-field electron microscopy (PINEM) [31], which originally operated in the visible and near-IR range [32–37]. The pulsed free electron interacts with the electric field along its trajectory, resulting in a widening of its energy spectrum. The image of the PhPs is produced when applying an energy filter that collects only the electrons that gained energy from their interaction with the PhPs. This technique is named energy-filtered transmission electron microscopy (EFTEM) [47–49]. The filtering creates a threshold for the minimum electric field that we can measure (1 MV/m; see Supplement 1, Section S1). Above this threshold, there is a quadratic connection between the integrated electric field along the electron trajectory and the number of counts in the image [32,33]. The dynamics of the field is probed when changing the time delay τ_d between the mid-IR pump pulse and the free-electron probe pulse. A similar approach to observe field spatiotemporal dynamics was first used in Ref. [43] to monitor the propagation of PhP wave packets and extract their group velocities. We use time steps of 50 fs and find vortex dynamics for a duration of 4.5 ps, significantly longer than the mid-IR pulse duration of 600 fs FWHM.

The PhP spatiotemporal dynamics is shown in Fig. 2(b) and Visualization 1. The PhP field is excited at the edges of the sample (coupling directly to the bulk is impossible due to momentum mismatch between free-space photons and PhP modes). From the edges, the PhP wave packets propagate toward the sample center ($\tau_d = 0$ to 0.4 ps) and interfere with each other (meeting at the center around $\tau_d = 0.6$ ps). Due to this interference, the measured field pattern fluctuates and changes in a complex manner. Yet, there are a few clear structures that stand out of this fluctuating landscape: nodal points and nodal lines in the PhP field. As shown by our simulations, these features are the signature of PhP vortices. That is, the interference of PhP wave packets that couple at the edges and reflect from them creates phase singularities observed as the nodal points in the field pattern. By following the nodal points inside these patterns, we study the vortex dynamics.

3. VORTEX CREATION AND ANNIHILATION

In Fig. 3 (and Visualization 2), we present an example of the simulated motion of vortex dynamics and their processes of creation and annihilation. This motion is predetermined given the dispersion relation, pump spectra, polarization, and direction, as well as sample boundary conditions (see thorough description in Supplement 1 Section S2). We simulate a $6 \times 6 \mu\text{m}^2$ square hBN sample and analyze both the amplitude and phase of the field in the time domain. Indeed, the nodal points of the field (top row) correspond to the optical vortices that we extract from the phase of the field (bottom row). By following the field map evolution in time, we find specific time stamps in which the vortices are created and annihilated. For further validation of the results, we also performed full electromagnetic COMSOL simulations of the field dynamics,

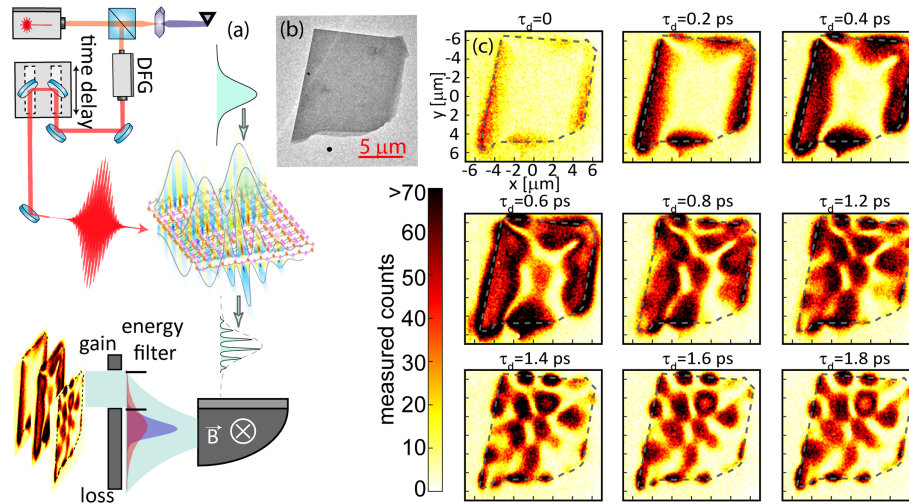


Fig. 2. Experimental setup and measurement examples showing spatiotemporal dynamics of optical vortices. (a) Experimental setup. A femtosecond laser pulse (orange) splits in two. One pulse serves as the pump, converted to the mid-infrared (IR; red) using difference frequency generation (DFG) and excites the phonon-polaritons (PhPs) in the sample. The other pulse is converted to ultraviolet (UV; purple) using fourth harmonic generation (FHG) and photoexcites the electron probe pulse (cyan). We image the PhP field in the hBN by energy filtering, counting only electrons that gained energy. The dynamics is retrieved by changing the time delay τ_d between the pump and the probe. (b) TEM image of the 40 nm thick isotopically pure hBN (^{10}B) sample. See Supplement 1, Section S3 and Fig. S4 for a detailed sample analysis. (c) PhP field patterns for different time delays, showing the evolution of complex interference pattern dynamics. The dashed gray contour is the sample's edge. The bright areas that include fewer counts are nodal lines and points where vortices are located. The full 3D movie that continues until $\tau_d = 4.5$ ps with 50 fs time steps can be found in Visualization 1.

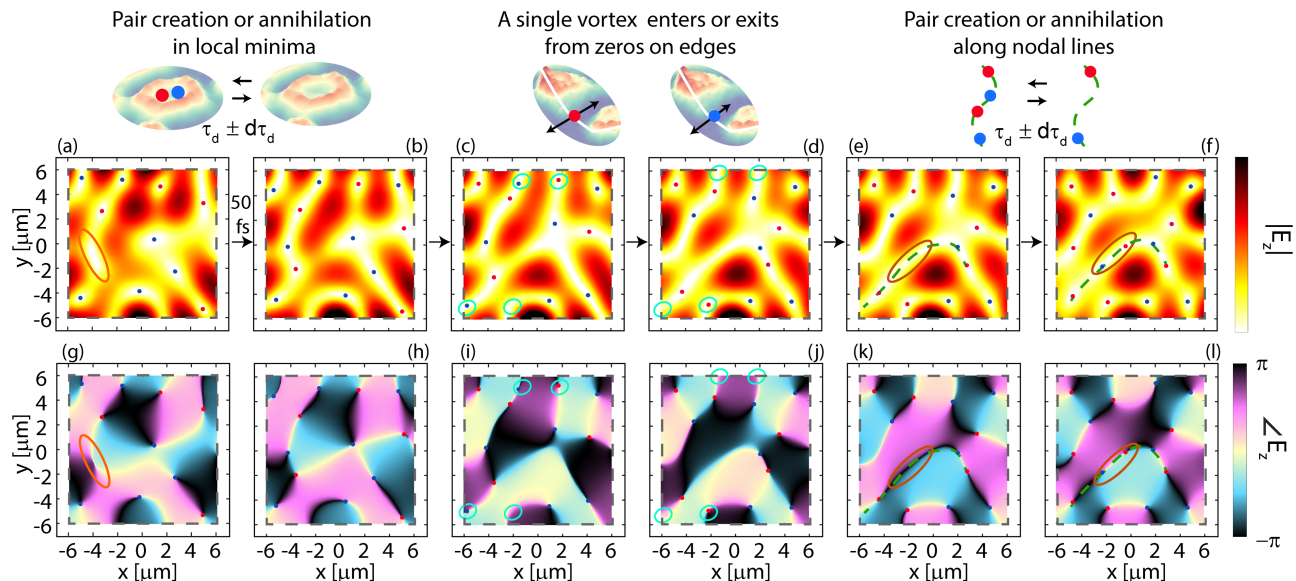


Fig. 3. Vortex dynamics, creation, and annihilation. (a), (b) A pair of right-handed and left-handed vortices can be created when the field amplitude at a certain point reduces to zero, forming a nodal point, or annihilated if the nodal point suddenly disappears. (c), (d) A single vortex of any orientation may be created or annihilated on the sample's edge. Thus, the sum of OAM over the entire sample is not conserved. (e), (f) A pair of vortices can be created or annihilated within nodal lines (dashed green) along which the field amplitude is already near zero. Such nodal lines are formed between at least two vortices with opposite orientations. Often when two vortices are distant from each other, additional vortex pairs are created between them, effectively supporting a longer nodal line. (g)–(l) Phase maps corresponding to (a)–(f). The time delay between consequent images is 50 fs.

showing that the measured features can be reproduced numerically for a sample shape similar to the one used in the experiment (Figs. S6 and S7).

Figure 3 summarizes the three mechanisms in which vortices are created and annihilated. The first option (Fig. 3 left column) is the creation of a pair of opposite sign vortices, occurring when the amplitude of a certain point reduces to zero. Accordingly, a non-zero local minimum possesses an OAM of zero but has the

potential to become the source of a pair of vortices (similar to exciton-polariton pair creation and annihilation [50]). When they move away from one another, they create a nodal line. Nodal lines appear as continuous curves along which the field is near zero. They are formed by a set of vortices of alternating OAM that destructively interferes.

The second option for the creation or annihilation of a pair of vortices is inside an existing nodal line (Fig. 3 right column).

When the distance between neighboring vortices inside a nodal line grows, another pair of vortices with opposite signs is often created along the nodal line, maintaining a longer nodal line through destructive interference. Importantly, in both of the above mechanisms of pair creation, each individual vortex can move inside the sample and annihilate with any vortex of the opposite OAM.

Since pairs of vortices can be created or annihilated, the total number of vortices is not conserved. The quantity that is conserved is the sum of OAM during interaction between vortices, defined by a closed-loop phase integration around a specific point where and when the interaction occurs. However, the sum of OAM of the sample, i.e., the phase integration along the sample's edge, is not conserved due to a third mechanism of vortex creation and annihilation—along the edges, single vortices can be created or annihilated (Fig. 3 middle column). At the core of this mechanism is the effect of anomalous reflection of planar waves at the edges of the sample that adds a phase to the field [41,51]. Altering the phase locally enables phase distortions equivalent to having single vortices enter and exit the sample along the edges. From a different point of view, because of the nature of optical vortices [1], the sum of the OAM of all vortices in the sample equals the integrated phase along the sample edges, and if the phase is changing, a vortex might be created or annihilated. Once a vortex is created on the sample

edge, it can change its location, annihilate with another vortex of opposite sign (as also shown in an exciton–polariton platform [50]), or annihilate on the edge (usually at a different location from where it was created).

4. ANALYSIS OF THE MEASURED SPATIOTEMPORAL VORTEX DYNAMICS

Our experimental observation of vortex creation and annihilation demonstrates the features predicted by theory. Specifically, Fig. 4(a) shows selected time frames to highlight vortex dynamics, in close agreement with the theory we show in Fig. 1: we follow the trajectories of all the vortices in the flake and find that certain trajectories of vortices of opposite signs can begin (end) at certain points in time and space, which corresponds to the process of creation (annihilation). The complete measurement including the locations and signs of the vortices in each time frame is shown in Visualization 3 and Fig. S1.

Figures 4(b)–(e) show how we deduce the location and sign of the vortices. For each frame, we find the vortex locations by identifying the nodal points and nodal lines, appearing as areas with extremely low counts [Fig. 4(b) and Fig. S2]. The resolution for determining the location of each vortex is typically

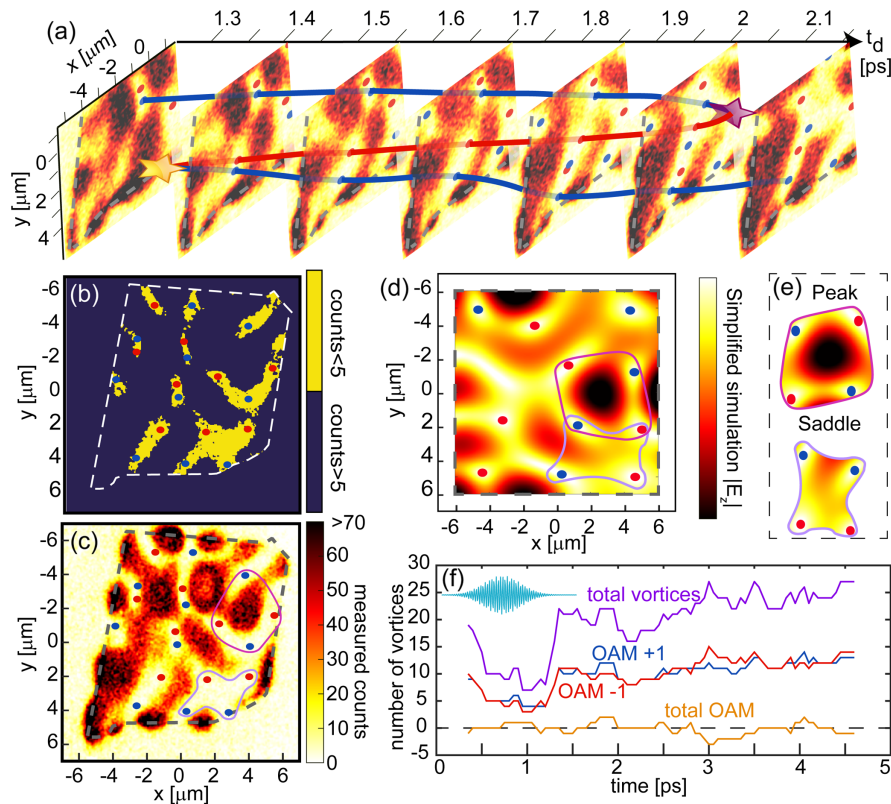


Fig. 4. Observation of vortex dynamics. (a) Selected time frames showing the vortex dynamics, marking events of creation and annihilation. A few vortex trajectories are shown through the blue and red curves: a right-handed (red) vortex is created from a pair creation process at $\tau_d = 1.3$ ps and annihilated with a left-handed (blue) vortex at $\tau_d = 2.05$ ps. The reconstruction of all vortices throughout our measurement is shown in Fig. S1 and Visualization 3. (b) First step for identification of vortices—areas of nodal points and nodal lines (where optical vortices appear) are denoted in yellow (more information in Fig. S2). (c) Experimental measurement for $\tau_d = 1.8$ ps with the estimated vortex locations (up to flipping all vortex orientations). (d) Simulation field pattern in a specific time frame, showing how a set of vortices can determine the qualitative shape of the field's pattern inside the sample. (e) An amplitude peak is formed when surrounded by a set of vortices with alternating orientations (pink). When the vortex orientations are not alternating, a saddle point is created, having a smaller amplitude compared to the peak (gray). (f) Number of vortices with an OAM of +1 (blue), -1 (red), their sum (purple), and difference (brown). The total OAM is not expected to be conserved due to creation or annihilation of vortices on the edges, while the total number of vortices includes pair creation or annihilation. The excitation pulse duration is shown in blue. The comparison with a full numerical COMSOL simulation is shown in Fig. S7 (see Visualization 4).

$100 \times 100 \text{ nm}^2$ (3×3 pixels). We analyze the field pattern to determine the OAM sign of each vortex [Fig. 4(c)]. Since we do not have a direct phase measurement, our overall vortex reconstruction relies on the time-domain dynamics and on identifying events of creation and annihilation. The remaining degree of freedom is indistinguishable: if all vortices flip their OAM, the amplitude map that we measure does not change (i.e., we could flip all vortices blue \leftrightarrow red). Another unknown quantity is the number of vortices found along each nodal line, since the near-zero amplitude along these lines can potentially sustain arbitrary numbers of degenerate vortices, where each pair has its phase cancelling out. To extract the exact phase at each point in time and space, additional advances in electron near-field measurement are required.

We can verify from simulations [Figs. 4(d) and 4(e)] the relative sign between the vortices. Each peak of the field is surrounded by a set of vortices of alternating signs (e.g., $+ - + -$), forcing a uniformity in the phase within the peak. In contrast, when vortices do not have alternating signs (e.g., $+ + - -$), the field surrounded by these vortices is not a peak but a saddle, having a smaller amplitude compared to a peak and a larger variation in the phase inside it. The saddle configuration can create a large area in the sample with very low counts [Fig. 4(c) bottom right]. This area seems to have almost zero counts due to the minimal electric field that we can measure, but it is not strictly zero (see the average signal over time, Fig. S3). Finally, when comparing the estimated vortices in all time stamps, we recognize the continuous movement of the vortices and the events of vortex creation and annihilation.

5. DISCUSSION AND OUTLOOK

Our experiment stands as an example for the universal nature of boundary-launched planar optical vortices. In most experiments that have shown planar optical vortices so far, the boundary conditions were designed for generating a specific vortex OAM at a specific location that remains constant in time (e.g., Refs. [21,22]). In our experiment, we used the natural edges of the sample to show

that vortex spatiotemporal dynamics can appear in arbitrary samples with only a single requirement—that the sample is optically mesoscopic. We can divide all samples into three categories (see Fig. 5). (1) If the sample's dimensions are smaller than the typical wavelength of the optical modes, it can support only a few modes. The fields in such cavity-like samples possess distinct shapes [41] and cannot show vortex dynamics or any complex dynamics. We present an example of such an observation in Fig. 5(a). The resonant mode can potentially have a phase singularity forming an optical vortex, but such a vortex cannot have temporal dynamics changing its location in time. (2) On the other extreme, if the sample's dimensions are much larger than the decay length of the optical modes (decay time multiplied by phase velocity), there is dynamics, but no interference from different boundaries, and thus optical vortices cannot form. This is the case in Ref. [43], shown in Fig. 5(c), having a wave packet propagating freely in-plane, moving away from the edge. (3) Consequently, spatiotemporal dynamics of vortices can occur only in samples of intermediate sizes—optically mesoscopic samples—larger than the typical wavelength of the optical modes and smaller than their typical decay length. This is the case in our work, as shown in Fig. 5(b).

It is interesting to compare the features of PhP vortices to those in exciton–polariton condensates [52]. There, a strong interaction between matter and an optical cavity mode creates the condensate, which can form a superfluid [53]. Previous work in such systems shows the creation and propagation of vortex pairs [50,54,55], including their spatiotemporal dynamics [30]. Although sharing certain polaritonic properties with PhPs, the behavior of exciton–polaritons arises from the Gross–Pitaevskii equation and requires extremely low temperatures, in contrast to the PhP vortices that arise from Maxwell's equations and were measured here at room temperature. Moreover, the degrees of freedom in designing the polariton vortices are completely different. While exciton–polariton vortices are determined by the external pump laser field profile [56–58], the van der Waals polariton dynamics is governed also by the boundary conditions (shape of the sample)

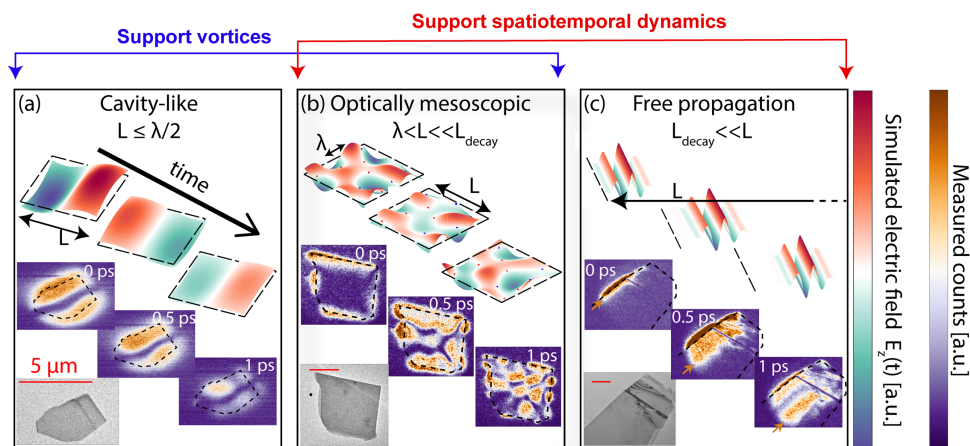


Fig. 5. Universality of boundary-launched optical vortex dynamics: planar optical vortices are expected in any mesoscopic-size sample of arbitrary shape. (a) Small samples: spatial dimensions (L) much smaller than the wavelength of light in the material (λ). The electric field pattern (both simulated and measured) has a cavity-like mode with no field dynamics. Such samples can support vortices for specific sample shapes, though the location of the vortex is static. (b) Optically mesoscopic samples: spatial dimensions (L) much smaller than the decay length of light in the material (L_{decay}) but larger than the wavelength of light in the material (λ). These conditions are sufficient for having the spatiotemporal dynamics of optical vortices (shown in both simulated and measured plots) in arbitrary sample shapes, due to complex interference patterns that evolve over time. (c) Large samples: spatial dimensions (L) much larger than the decay length of light in the material (L_{decay}). Such dimensions support free-propagation dynamics (data taken from Ref. [43]), until the field disperses and decays. In all figures, the dashed lines denote the sample's boundaries. The inset at the bottom of each panel shows a hBN flake of the corresponding size with which the presented data were collected. The red bar denotes $5 \mu\text{m}$ in all insets.

and by the PhP tunable dispersion relation, which strongly depend on the sample thickness and surrounding materials [45,46,59]. For example, thicker samples are expected to support fewer vortices due to the longer wavelength, creating a simpler vortex pattern and dynamics.

The properties of polaritons in van der Waals materials, combined with their slow group and phase velocities, and long lifetimes, create a unique opportunity for simulating and probing universal vortex phenomena in this platform. For example, recent demonstrations of quantum simulations [60] and analogies of gravity [61] with exciton–polaritons raise intriguing possibilities for similar prospects with PhPs, especially once higher excitation intensities unlock their nonlinear optical response [62]. Potentially, these vortex phenomena could be observed for surface-plasmon polaritons in metals, if probed with sufficiently short time resolutions [63]. It is possible that nonlinear effects had already affected our measurements here (see Fig. S8 and Supplement 1 Section S4). Future investigations may deliberately introduce nonlinearity through atomic emitters or 2D quantum wells, exploiting their extremely strong light–matter interactions with 2D light [64], and specifically with vortices of van der Waals polaritons [16,17].

In our measurement [Fig. 4(f)] and simulations (Fig. S7), we identify the total number of vortices and the total OAM of the flake as a function of time. We observe that the laser excitation [cyan in Fig. 4(f)] acts as a source of order that reduces the total number of vortices when it is applied on the sample, analogous to reducing the effective temperature in a solid-state BKT-type system. The number of vortices then gradually increases again after the laser excitation is over, since the entropy is increasing (forcing the scarcity of pair-annihilation processes compared to pair-creation). Moreover so, a wide range of vortex phenomena can be reached by engineering the sample's boundary conditions, such as using inverse design methods [65]. For example, a properly designed boundary condition could establish full entanglement between two vortex states of opposite charge (± 1) at two different locations r_1, r_2 : taking the form of $|+1, r_1\rangle|-1, r_2\rangle + |-1, r_1\rangle|+1, r_2\rangle$. Altogether, the freedoms in excitation pulses, sample shape, and dispersion relations make van der Waals materials an attractive platform for demonstrating and probing a wide range of vortex phenomena in optics and condensed matter physics.

Funding. European Research Council (726001); Office of Naval Research (N00014-22-1-2582); HORIZON EUROPE European Research Council (820378, 881603, 851780-ERC-NanoEP); Israel Science Foundation (830/19); Gobierno de España (PID2019-106875GB-I00, Severo Ochoa CEX2019-000910-S [MCIN/AEI/10.13039/501100011033]); Agencia Estatal de Investigación (PCI2021-122020-2A); European Union Next Generation EU/PRTR (PRTR-C17.I1); Fundació Cellex; Fundació Mir-Puig; Generalitat de Catalunya (CERCA, AGAUR, 2021 SGR 01443).

Acknowledgment. F.H.L.K. acknowledges support from the ERC, the government of Spain, the European Union Next Generation EU/PRTR, Fundació Cellex, Fundació Mir-Puig, and Generalitat de Catalunya. Furthermore, the research leading to these results has received funding from the European Union's Horizon 2020. H.H.S. acknowledges funding from the European Union's Horizon 2020 programme under the Marie Skłodowska-Curie grant agreement Ref. 843830.

Disclosures. The authors declare no conflicts of interest.

Data availability. Data underlying the results presented in this paper are not publicly available at this time but may be obtained from the authors upon reasonable request.

Supplemental document. See Supplement 1 for supporting content.

REFERENCES

1. J. F. Nye and M. V. Berry, "Dislocations in wave trains," *Proc. R. Soc. London A* **336**, 165–190 (1974).
2. L. D. P. Thibouque and P. Valrose, "Optical vortex," *Opt. Commun.* **73**, 403–408 (1989).
3. M. S. Soskin, V. N. Gorshkov, M. V. Vasnetsov, J. T. Malos, and N. R. Heckenberg, "Topological charge and angular momentum of light beams carrying optical vortices," *Phys. Rev. A* **56**, 4064–4075 (1997).
4. L. Allen, M. W. Beijersbergen, R. J. C. Spreeuw, and J. P. Woerdman, "Orbital angular momentum of light and the transformation of Laguerre-Gaussian laser modes," *Phys. Rev. A* **45**, 8185–8189 (1992).
5. Y. Gorodetski, A. Niv, V. Kleiner, and E. Hasman, "Observation of the spin-based plasmonic effect in nanoscale structures," *Phys. Rev. Lett.* **101**, 043903 (2008).
6. Y. Shen, X. Wang, Z. Xie, C. Min, X. Fu, Q. Liu, M. Gong, and X. Yuan, "Optical vortices 30 years on: OAM manipulation from topological charge to multiple singularities," *Light Sci. Appl.* **8**, 90 (2019).
7. K. I. Willig, S. O. Rizzoli, V. Westphal, R. Jahn, and S. W. Hell, "STED microscopy reveals that synaptotagmin remains clustered after synaptic vesicle exocytosis," *Nature* **440**, 935–939 (2006).
8. K. T. Gahagan and G. A. Swartzlander, "Optical vortex trapping of particles," *Opt. Lett.* **21**, 827–829 (1996).
9. G. A. Swartzlander and C. T. Law, "Optical vortex solitons observed in Kerr nonlinear media," *Phys. Rev. Lett.* **69**, 2503–2506 (1992).
10. E. Nagali, F. Sciarrino, F. De Martini, L. Marrucci, B. Piccirillo, E. Karimi, and E. Santamato, "Quantum information transfer from spin to orbital angular momentum of photons," *Phys. Rev. Lett.* **103**, 013601 (2009).
11. T. Stav, A. Faerman, E. Maguid, D. Oren, V. Kleiner, E. Hasman, and M. Segev, "Quantum entanglement of the spin and orbital angular momentum of photons using metamaterials," *Science* **361**, 1101–1104 (2018).
12. H. He, M. E. J. Friese, N. R. Heckenberg, and H. Rubinsztein-Dunlop, "Direct observation of transfer of angular momentum to absorptive particles from a laser beam with a phase singularity," *Phys. Rev. Lett.* **75**, 826–829 (1995).
13. M. L. M. Balistreri, J. P. Korterik, L. Kuipers, and N. F. van Hulst, "Local observations of phase singularities in optical fields in waveguide structures," *Phys. Rev. Lett.* **85**, 294–297 (2000).
14. K. Wang, E. Schonbrun, P. Steinvurzel, and K. B. Crozier, "Trapping and rotating nanoparticles using a plasmonic nano-tweezer with an integrated heat sink," *Nat. Commun.* **2**, 469 (2011).
15. S. Tsesses, E. Ostrovsky, K. Cohen, B. Gjonaj, N. H. Lindner, and G. Bartal, "Optical skyrmion lattice in evanescent electromagnetic fields," *Science* **361**, 993–996 (2018).
16. F. Machado, N. Rivera, H. Buljan, M. Soljačić, and I. Kaminer, "Shaping polaritons to reshape selection rules," *ACS Photon.* **5**, 3064–3072 (2018).
17. J. Sloan, N. Rivera, J. D. Joannopoulos, I. Kaminer, and M. Soljačić, "Controlling spins with surface magnon polaritons," *Phys. Rev. B* **100**, 30–33 (2019).
18. H. Kim, J. Park, S. W. Cho, S. Y. Lee, M. Kang, and B. Lee, "Synthesis and dynamic switching of surface plasmon vortices with plasmonic vortex lens," *Nano Lett.* **10**, 529–536 (2010).
19. A. David, B. Gjonaj, Y. Blau, S. Dolev, and G. Bartal, "Nanoscale shaping and focusing of visible light in planar metal–oxide–silicon waveguides," *Optica* **2**, 1045–1048 (2015).
20. E. Ostrovsky, K. Cohen, S. Tsesses, B. Gjonaj, and G. Bartal, "Nanoscale control over optical singularities," *Optica* **5**, 283–288 (2018).
21. G. Spektor, E. Prinz, M. Hartelt, A. K. Mahro, M. Aeschlimann, and M. Orenstein, "Orbital angular momentum multiplication in plasmonic vortex cavities," *Sci. Adv.* **7**, eabg5571 (2021).
22. G. Spektor, D. Kilbane, A. K. Mahro, B. Frank, S. Ristok, L. Gal, P. Kahl, D. Podbiel, S. Mathias, H. Giessen, F.-J. Meyer zu Heringdorf, M. Orenstein, and M. Aeschlimann, "Revealing the subfemtosecond dynamics of orbital angular momentum in nanoplasmonic vortices," *Science* **355**, 1187–1191 (2017).
23. Y. Dai, Z. Zhou, A. Ghosh, R. S. K. Mong, A. Kubo, C. Bin Huang, and H. Petek, "Plasmonic topological quasiparticle on the nanometre and femtosecond scales," *Nature* **588**, 616–619 (2020).
24. T. J. Davis, D. Janoschka, P. Dreher, B. Frank, F. J. Meyer zu Heringdorf, and H. Giessen, "Ultrafast vector imaging of plasmonic skyrmion dynamics with deep subwavelength resolution," *Science* **368**, eaba6415 (2020).

25. M. V. Berry and M. R. Dennis, "Knotted and linked phase singularities in monochromatic waves," *Proc. R. Soc. A Math. Phys. Eng. Sci.* **457**, 2251–2263 (2001).
26. L. De Angelis, F. Alpeggiani, A. Di Falco, and L. Kuipers, "Spatial distribution of phase singularities in optical random vector waves," *Phys. Rev. Lett.* **117**, 093901 (2016).
27. L. De Angelis, F. Alpeggiani, A. Di Falco, and L. Kuipers, "Persistence and lifelong fidelity of phase singularities in optical random waves," *Phys. Rev. Lett.* **119**, 203903 (2017).
28. J. M. Kosterlitz and D. J. Thouless, "Ordering, metastability and phase transitions in two-dimensional systems," *J. Phys. C* **6**, 1181–1203 (1973).
29. S. J. DeCamp, G. S. Redner, A. Baskaran, M. F. Hagan, and Z. Dogic, "Orientational order of motile defects in active nematics," *Nat. Mater.* **14**, 1110–1115 (2015).
30. L. Dominici, G. Dagvadorj, J. M. Fellows, D. Ballarini, M. De Giorgi, F. M. Marchetti, B. Piccirillo, L. Marrucci, A. Bramati, G. Gigli, M. H. Szymańska, and D. Sanvitto, "Vortex and half-vortex dynamics in a nonlinear spinor quantum fluid," *Sci. Adv.* **1**, e1500807 (2015).
31. B. Barwick, D. J. Flannigan, and A. H. Zewail, "Photon-induced near-field electron microscopy," *Nature* **462**, 902–906 (2009).
32. F. J. Garcia De Abajo, A. Asenjo-Garcia, and M. Kociak, "Multiphoton absorption and emission by interaction of swift electrons with evanescent light fields," *Nano Lett.* **10**, 1859–1863 (2010).
33. S. T. Park, M. Lin, and A. H. Zewail, "Photon-induced near-field electron microscopy (PINEM): theoretical and experimental," *New J. Phys.* **12**, 123028 (2010).
34. T. T. A. Lummen, R. J. Lamb, G. Berruto, T. Lagrange, L. Dal Negro, F. J. Garcia De Abajo, D. McGrouther, B. Barwick, and F. Carbone, "Imaging and controlling plasmonic interference fields at buried interfaces," *Nat. Commun.* **7**, 13156 (2016).
35. E. Pomarico, I. Madan, G. Berruto, G. M. Vanacore, K. Wang, I. Kaminer, F. J. Garcia De Abajo, and F. Carbone, "MeV resolution in laser-assisted energy-filtered transmission electron microscopy," *ACS Photon.* **5**, 759–764 (2018).
36. I. Madan, G. M. Vanacore, E. Pomarico, G. Berruto, R. J. Lamb, D. McGrouther, T. T. A. Lummen, T. Latychevskaia, F. J. Garcia De Abajo, and F. Carbone, "Holographic imaging of electromagnetic fields via electron-light quantum interference," *Sci. Adv.* **5**, eaav8358 (2019).
37. K. Wang, R. Dahan, M. Shentcis, Y. Kauffmann, A. Ben Hayun, O. Reinhardt, S. Tseses, and I. Kaminer, "Coherent interaction between free electrons and a photonic cavity," *Nature* **582**, 50–54 (2020).
38. S. Dai, Z. Fei, Q. Ma, A. S. Rodin, M. Wagner, A. S. McLeod, M. K. Liu, W. Gannett, W. Regan, K. Watanabe, T. Taniguchi, M. Thiemens, G. Dominguez, A. H. Castro Neto, A. Zettl, F. Keilmann, P. Jarillo-Herrero, M. M. Fogler, and D. N. Basov, "Tunable phonon polaritons in atomically thin van der Waals crystals of boron nitride," *Science* **343**, 1125–1129 (2014).
39. J. D. Caldwell, A. V. Kretinin, Y. Chen, V. Giannini, M. M. Fogler, Y. Francescato, C. T. Ellis, J. G. Tischler, C. R. Woods, A. J. Giles, M. Hong, K. Watanabe, T. Taniguchi, S. A. Maier, and K. S. Novoselov, "Sub-diffractive volume-confined polaritons in the natural hyperbolic material hexagonal boron nitride," *Nat. Commun.* **5**, 5221 (2014).
40. A. J. Giles, S. Dai, I. Vurgaftman, T. Hoffman, S. Liu, L. Lindsay, C. T. Ellis, N. Assefa, I. Chatzakis, T. L. Reinecke, J. G. Tischler, M. M. Fogler, J. H. Edgar, D. N. Basov, and J. D. Caldwell, "Ultralow-loss polaritons in isotopically pure boron nitride," *Nat. Mater.* **17**, 134–139 (2018).
41. M. Tamagnone, A. Ambrosio, K. Chaudhary, L. A. Jauregui, P. Kim, W. L. Wilson, and F. Capasso, "Ultra-confined mid-infrared resonant phonon polaritons in van der Waals nanostructures," *Sci. Adv.* **4**, 4–10 (2018).
42. K. Chaudhary, M. Tamagnone, M. Rezaee, D. K. Bediako, A. Ambrosio, P. Kim, and F. Capasso, "Engineering phonon polaritons in van der Waals heterostructures to enhance in-plane optical anisotropy," *Sci. Adv.* **5**, eaau7171 (2019).
43. Y. Kurman, R. Dahan, H. H. Sheinfux, K. Wang, M. Yannai, Y. Adiv, O. Reinhardt, L. H. G. Tizei, S. Y. Woo, J. Li, J. H. Edgar, M. Kociak, F. H. L. Koppens, and I. Kaminer, "Spatiotemporal imaging of 2D polariton wave packet dynamics using free electrons," *Science* **372**, 1181–1186 (2021).
44. G. Pavlidis, J. J. Schwartz, J. Matson, T. Folland, S. Liu, J. H. Edgar, J. D. Caldwell, and A. Centrone, "Experimental confirmation of long hyperbolic polariton lifetimes in monoisotopic (10B) hexagonal boron nitride at room temperature," *APL Mater.* **9**, 091109 (2021).
45. D. N. Basov, M. M. Fogler, and F. J. Garcia de Abajo, "Polaritons in van der Waals materials," *Science* **354**, aag1992 (2016).
46. T. Low, A. Chaves, J. D. Caldwell, A. Kumar, N. X. Fang, P. Avouris, T. F. Heinz, F. Guinea, L. Martin-Moreno, and F. Koppens, "Polaritons in layered 2D materials," *Nat. Mater.* **16**, 182–194 (2016).
47. R. F. Egerton, *Electron Energy-Loss Spectroscopy in the Electron Microscope* (Springer US, 2011).
48. J. Nelayah, M. Kociak, O. Stéphan, F. J. G. De Abajo, M. Tencé, L. Henrard, D. Taverna, I. Pastoriza-Santos, L. M. Liz-Marzán, and C. Colliex, "Mapping surface plasmons on a single metallic nanoparticle," *Nat. Phys.* **3**, 348–353 (2007).
49. M. Bosman, V. J. Keast, M. Watanabe, A. I. Maarroof, and M. B. Cortie, "Mapping surface plasmons at the nanometre scale with an electron beam," *Nanotechnology* **18**, 165505 (2007).
50. L. Dominici, N. Voronova, D. Colas, A. Gianfrate, A. Rahmani, V. Ardizzone, D. Ballarini, M. De Giorgi, G. Gigli, F. P. Laussy, and D. Sanvitto, "Shaping the topology of light with a moving Rabi-oscillating vortex," *Opt. Express* **29**, 37262–37280 (2021).
51. J. H. Kang, S. Wang, Z. Shi, W. Zhao, E. Yablonovitch, and F. Wang, "Goos-Hänchen shift and even-odd peak oscillations in edge-reflections of surface polaritons in atomically thin crystals," *Nano Lett.* **17**, 1768–1774 (2017).
52. K. G. Lagoudakis, M. Wouters, M. Richard, A. Baas, I. Carusotto, R. André, L. S. Dang, and B. Deveaud-Plédran, "Quantized vortices in an exciton-polariton condensate," *Nat. Phys.* **4**, 706–710 (2008).
53. A. Amo, J. Lefrère, S. Pigeon, C. Adrados, C. Ciuti, I. Carusotto, R. Houdré, E. Giacobino, and A. Bramati, "Superfluidity of polaritons in semiconductor microcavities," *Nat. Phys.* **5**, 805–810 (2009).
54. A. Amo, S. Pigeon, D. Sanvitto, V. G. Sala, R. Hivet, I. Carusotto, F. Pisanello, G. Leménager, R. Houdré, E. Giacobino, C. Ciuti, and A. Bramati, "Polariton superfluids reveal quantum hydrodynamic solitons," *Science* **332**, 1167–1170 (2011).
55. G. Lerario, A. Maître, R. Boddeda, Q. Glorieux, E. Giacobino, S. Pigeon, and A. Bramati, "Vortex-stream generation and enhanced propagation in a polariton superfluid," *Phys. Rev. Res.* **2**, 1–5 (2020).
56. F. M. Marchetti, M. H. Szymańska, C. Tejedor, and D. M. Whittaker, "Spontaneous and triggered vortices in polariton optical-parametric-oscillator superfluids," *Phys. Rev. Lett.* **105**, 1–4 (2010).
57. G. Tosi, G. Christmann, N. G. Berloff, P. Tsotsis, T. Gao, Z. Hatzopoulos, P. G. Savvidis, and J. J. Baumberg, "Geometrically locked vortex lattices in semiconductor quantum fluids," *Nat. Commun.* **3**, 1–5 (2012).
58. T. Boulier, H. Terças, D. D. Solnyshkov, Q. Glorieux, E. Giacobino, G. Malpuech, and A. Bramati, "Vortex chain in a resonantly pumped polariton superfluid," *Sci. Rep.* **5**, 9230 (2015).
59. H. H. Sheinfux, L. Orsini, M. Jung, I. Torre, M. Ceccanti, R. Maniyara, D. B. Ruiz, A. Hötger, R. Bertini, S. Castilla, N. C. H. Hesp, E. Janzen, A. Holleitner, V. Pruneri, J. H. Edgar, G. Shvets, and F. H. L. Koppens, "Multimodal interference and bound in the continuum modes in indirectly-patterned hyperbolic cavities," *arXiv*, arXiv:2202.08611 (2022).
60. T. Boulier, M. J. Jacquet, A. Maître, G. Lerario, F. Claude, S. Pigeon, Q. Glorieux, A. Amo, J. Bloch, A. Bramati, and E. Giacobino, "Microcavity polaritons for quantum simulation," *Adv. Quantum Technol.* **3**, 2000052 (2020).
61. M. J. Jacquet, T. Boulier, F. Claude, A. Maître, E. Cancellieri, C. Adrados, A. Amo, S. Pigeon, Q. Glorieux, A. Bramati, and E. Giacobino, "Polariton fluids for analogue gravity physics: polariton fluids for analogue gravity," *Philos. Trans. R. Soc. A* **378**, 1–18 (2020).
62. F. Iyikanat, A. Konečná, and F. J. G. De Abajo, "Nonlinear tunable vibrational response in hexagonal boron nitride," *ACS Nano* **15**, 13415–13426 (2021).
63. A. Losquin and T. T. A. Lummen, "Electron microscopy methods for space-, energy-, and time-resolved plasmonics," *Front. Phys.* **12**, 127301 (2017).
64. Y. Kurman and I. Kaminer, "Tunable bandgap renormalization by non-local ultra-strong coupling in nanophotonics," *Nat. Phys.* **16**, 868–874 (2020).
65. A. Y. Piggott, J. Lu, K. G. Lagoudakis, J. Petykiewicz, T. M. Babinec, and J. Vucković, "Inverse design and demonstration of a compact and broadband on-chip wavelength demultiplexer," *Nat. Photonics* **9**, 374–377 (2015).